VITOR DIEGO DIAS ENGERS

ALGORITMOS DE PREDIÇÃO PARA RÁDIO-OCULTAÇÃO EM CUBESATS: IMPLEMENTAÇÃO E COMPARATIVO ENTRE PLATAFORMAS FPGA E MICROCONTROLADOR

Joinville

2025

VITOR DIEGO DIAS ENGERS

ALGORITMOS DE PREDIÇÃO PARA RÁDIO-OCULTAÇÃO EM CUBESATS: IMPLEMENTAÇÃO E COMPARATIVO ENTRE PLATAFORMAS FPGA E MICROCONTROLADOR

UNIVERSIDADE FEDERAL DE SANTA CATARINA

CENTRO TECNOLÓGICO DE JOINVILLE

PROGRAMA DE PÓS-GRADUAÇÃO EM ENGENHARIA DE SISTEMAS ELETRÔNICOS

Orientador: Prof. Bezerra, Dr

Joinville

2025

VITOR DIEGO DIAS ENGERS
ALGORITMOS DE PREDIÇÃO PARA RÁDIO-OCULTAÇÃO EM CUBESATS: IMPLEMENTAÇÃO E COMPARATIVO ENTRE PLATAFORMAS FPGA E MICRO-CONTROLADOR/ VITOR DIEGO DIAS ENGERS. – Joinville, 2025-
43p. : il. (algumas color.) ; 30 cm.

Orientador: Prof. Bezerra, Dr

Dissertação (Mestrado) – UNIVERSIDADE FEDERAL DE SANTA CATARINA
CENTRO TECNOLÓGICO DE JOINVILLE
PROGRAMA DE PÓS-GRADUAÇÃO EM ENGENHARIA DE SISTEMAS ELETRÔNICOS, 2025.

1. Engenharia de Sistemas Eletrônicos. 2. Caracterização de Impedância Térmica. 3. Confiabilidade de Módulos IGBT. I. Santos Greff, Diego. II. Universidade Federal de Santa Catarina. III. Título.

VITOR DIEGO DIAS ENGERS

ALGORITMOS DE PREDIÇÃO PARA RÁDIO-OCULTAÇÃO EM CUBESATS: IMPLEMENTAÇÃO E COMPARATIVO ENTRE PLATAFORMAS FPGA E MICROCONTROLADOR

O presente trabalho em nível de Mestrado foi avaliado e aprovado, em 18 de dezembro de 2024, pela banca examinadora composta pelos seguintes membros:

Prof. Bezerra, Dr
Orientador

Sergio Vidal Garcia Oliveira
UDESC

Allan Fagner Cupertino
UFJF

Joinville
2025

Este trabalho é dedicado aos meus queridos pais.

AGRADECIMENTOS

Primeiramente, agradeço a Deus, por me agraciar com paz, saúde, serenidade e determinação ao longo desta jornada.

Aos meus pais, pelo apoio e incentivo incondicional em todas as etapas da minha trajetória.

Ao meu orientador, professor Dr. Diego Santos Greff, pela paciência, esclarecer minhas dúvidas ao longo deste estudo, e por constantemente me desafiar.

À WEG, por incentivar seus colaboradores a se desenvolverem profissionalmente.

Ao Itamar Fernandes Soares, pelas inúmeras discussões e sugestões durante a execução da pesquisa.

Ao Odilgei Hess Gonçalves, pelas valiosas contribuições, sugestões e discussões realizadas durante a execução dos experimentos.

Aos amigos Tiago Lemes da Silva, Odair da Rosa, Márcio Denilson Bouldann, Leandro Fisch e Mateus Abreu de Andrade, pelo apoio constante ao longo desta jornada do mestrado.

A todos que, de forma direta ou indireta, contribuíram para a concepção desta dissertação.

À Roberta, pela revisão do texto.

"Estejam vigilantes, mantenham-se firmes na fé, sejam homens de coragem, sejam fortes."
(1 Coríntios 16:13)

RESUMO

Esta dissertação investiga métodos para medir a impedância térmica em módulos IGBT, com foco na análise de confiabilidade, identificação de falhas e desempenho térmico. São discutidos os principais modos de falha, os tipos de encapsulamento e a relevância dos ensaios de vida acelerada na avaliação de módulos IGBT. Simulações baseadas na variação dos parâmetros do modelo de Foster foram realizadas para representar a degradação do encapsulamento, avaliando seus impactos na temperatura virtual de junção, na impedância térmica e na função estrutural cumulativa. Os resultados ajudam a identificar áreas críticas de potencial falha. No âmbito experimental, foram realizadas medições da temperatura virtual de junção e comparações entre os métodos estático e dinâmico para a determinação da impedância térmica, ambos apresentando resultados consistentes. O estudo enfatiza a necessidade de considerar a não linearidade da condutância térmica em função da temperatura, fundamental para análises precisas. Adicionalmente, são comparados dois métodos de medição da impedância térmica entre a junção e o case em módulos de potência sem baseplate: o método estático, que monitora a curva de resfriamento após a aplicação de um pulso prolongado de potência, e o método dinâmico, baseado na aplicação sucessiva de pulsos de potência de diferentes larguras.

Palavras-chave: Caracterização de Impedância Térmica; Confiabilidade de Módulos IGBT; Medição de Temperatura Virtual de Junção; Análise de Função Estrutural Cumulativa; Método de Medição Estático; Método de Medição Dinâmico.

ABSTRACT

This dissertation investigates methods for measuring thermal impedance in IGBT modules, focusing on reliability analysis, fault identification, and thermal performance. The main failure modes, encapsulation types, and the relevance of accelerated lifetime testing for IGBT modules are discussed. Simulations based on variations in Foster model parameters were conducted to represent encapsulation degradation, assessing its impacts on virtual junction temperature, thermal impedance, and cumulative structural function. The results contribute to identifying critical areas of potential failure. On the experimental side, virtual junction temperature measurements were carried out, along with comparisons between static and dynamic methods for determining thermal impedance, both yielding consistent results. The study highlights the importance of accounting for the nonlinearity of thermal conductance as a function of temperature, which is essential for accurate analyses. Additionally, two methods for measuring thermal impedance between the junction and the case in baseplate-less power modules are compared: the static method, which monitors the cooling curve after applying a prolonged power pulse, and the dynamic method, based on successive power pulses of varying widths.

Keywords: Thermal Impedance Characterization; Reliability of IGBT Modules; Virtual Junction Temperature Measurement; Cumulative Structure Function Analysis; Static Measurement Method; Dynamic Measurement Method.

LISTA DE ILUSTRAÇÕES

Figura 1 – Schematic geometry of a GNSS radio occultation event. The transmitted signal from the GNSS satellite is refracted as it passes through the atmosphere, arriving at the LEO receiver with a bending angle α. The tangent point represents the lowest altitude reached by the ray path. Adapted from (KURSINSKI et al., 1997). 32

LISTA DE TABELAS

Tabela 1 – Overview of major GNSS-RO missions and CubeSat constellations. . . 36

LISTA DE ABREVIATURAS E SIGLAS

MOSFET	Metal Oxide Semiconductor Field Effect Transistor
IGBT	Insulated Gate Bipolar Transistor
HVDC	High Voltage Direct Current
CTE	Coefficient of Thermal Expansion
DBC	Direct Bonded Copper
FDP	Função Densidade de Probabilidade
FDA	Função de Distribuição Acumulada
FEC	Função Estrutural Cumulativa
DUT	Device under test
TSEP	Temperature sensitive electrical parameters
NTC	Coeficiente de Temperatura Negativo
PTC	Coeficiente de Temperatura Positivo

LISTA DE SÍMBOLOS

P_T	Perdas Totais
E_{on}	Energia dissipada ao ligar o IGBT
E_{off}	Energia dissipada ao desligar o IGBT
P_{ch}	Perdas por comutação
P_{cond}	Perdas por condução
T_{vjmax}	Temperatura Virtual de Junção Máxima
Δl	Variação do comprimento
l_0	Comprimento inicial
ΔT	Variação de Temperatura
β	Fator de forma
α	Fator de escala
λ	Taxa de falha
FA	Fator de Aceleração
T_{op}	Tempo de Operação
T_{ac}	Tempo de ensaio acelerado
N_f	Número de ciclos até a falha
k_1	Constante de ajuste da curva
k_2	Constante de ajuste da curva
E_a	Energia de ativação
k_b	Constante de Boltazmann
C	Contante de proporcionalidade
T_{jm}	Temperatura Média de Junção
t_{on}	Tempo de acionamento do interruptor

D	Diâmetro do fio
I	Corrente por fio
V	Tensão sobre o interruptor
R_{th}	Resistência térmica
λ_{th}	Condutividade térmica
A	Área
d	Espessura
C_{th}	Capacitância térmica
c	Capacidade térmica do material
ρ	Densidade do material
T_{vj}	Temperatura Virtual de Junção
T_c	Temperatura de Case
T_h	Temperatura do Dissipador
I_C	Corrente de Coletor
Z_{thJC}	Impedância Térmica entre Junção e o Case
Z_{thJH}	Impedância Térmica entre Junção e o Dissipador
Z_{th}	Impedância Térmica
τ_{th}	Constante térmica
$R(\tau)$	Espectro de constante de tempo
$R_{th\Sigma}$	Resistência térmica acumulada
$C_{th\Sigma}$	Capacitância térmica acumulada
V_{cesat}	Tensão entre coletor e emissor no estado de condução
$\alpha_{calibração}$	Coeficiente de calibração mV/°C
T_{vj0}	Temperatura Virtual de Junção inicial
t_d	Tempo de atraso

SUMÁRIO

1 INTRODUCTION . . . 25
1.1 THE CUBESAT REVOLUTION IN ATMOSPHERIC OBSERVATION 25
1.2 MOTIVATION: EMBEDDED ALGORITHMS FOR CUBESAT RO . 26
1.3 OBJECTIVES . . . 27
1.3.1 General Objective . . . 27
1.3.2 Specific Objectives . . . 27
1.4 CONTRIBUTIONS . . . 28
1.5 DOCUMENT STRUCTURE . . . 28

2 METHODOLOGY . . . 29
2.1 Overview of the Radio Occultation Technique . . . 29
2.2 CubeSat Platforms for Radio Occultation . . . 30
2.2.1 Commercial CubeSat Constellations . . . 30
2.2.2 Advantages and Challenges of CubeSat RO . . . 31
2.3 Geometry of GNSS Radio Occultation Measurements . . . 32
2.4 Signal Processing and Bending Angle Retrieval . . . 33
2.4.1 GNSS Signal Tracking . . . 33
2.4.2 Excess Phase and Doppler Derivation . . . 34
2.4.3 Derivation of Bending Angle from Doppler . . . 34
2.4.4 Ionospheric Correction . . . 34
2.5 Inversion from Bending Angle to Atmospheric Profiles . . . 35
2.5.1 The Abel Transform . . . 35
2.5.2 Retrieval of Temperature, Pressure, and Humidity . . . 35
2.5.3 Ionospheric Electron Density Retrieval . . . 36
2.6 Data Sources and Pre-processing . . . 36
2.7 Quality Control and Error Characterization . . . 37
2.7.1 Error Sources in GNSS-RO . . . 37
2.8 Validation Approach . . . 38
2.8.1 Radiosonde Comparisons . . . 38
2.8.2 Reanalysis and NWP Comparisons . . . 38
2.8.3 Inter-Satellite Comparisons . . . 39
2.8.4 Self-Consistency Tests . . . 39
2.9 Summary . . . 39

REFERÊNCIAS . . . 41

1 INTRODUCTION

The observation and prediction of atmospheric conditions are fundamental to a wide range of societal activities, from weather forecasting and aviation safety to climate monitoring and disaster preparedness. Among the remote sensing techniques that have emerged over the past three decades, **radio occultation** (RO) has established itself as a uniquely valuable method for profiling the Earth's atmosphere with high vertical resolution, global coverage, and long-term stability (KURSINSKI et al., 1997; ANTHES, 2011).

Radio occultation exploits the refraction of radio signals from Global Navigation Satellite Systems (GNSS), such as GPS, Galileo, and GLONASS, as these signals traverse the atmosphere on their way to receivers aboard Low Earth Orbit (LEO) satellites. The bending and delay of the signals encode information about the atmospheric refractive index, which can be inverted to retrieve vertical profiles of temperature, pressure, humidity, and electron density (HAJJ et al., 2002). Unlike optical and infrared sensors, GNSS-RO measurements are unaffected by clouds and precipitation, providing reliable observations under all weather conditions.

The technique has proven particularly impactful for numerical weather prediction (NWP), where RO observations have been identified as one of the most cost-effective data sources per observation for improving forecast accuracy, especially in data-sparse regions such as the Southern Hemisphere oceans and polar areas (CUCURULL et al., 2007; POLI; HEALY; DEE, 2010). Furthermore, the inherent calibration stability of GNSS signals—traceable to atomic frequency standards—makes RO data an essential component of climate monitoring systems (STEINER et al., 2013).

1.1 THE CUBESAT REVOLUTION IN ATMOSPHERIC OBSERVATION

Traditionally, GNSS-RO missions have relied on large, expensive satellite platforms developed by governmental space agencies. Missions such as CHAMP (2000), GRACE (2002), and COSMIC/FORMOSAT-3 (2006) demonstrated the scientific and operational value of RO, but their high costs and long development cycles limited the number of deployed receivers and, consequently, the spatial and temporal density of observations (ANTHES et al., 2008; WICKERT et al., 2001).

The emergence of **CubeSat technology** has fundamentally transformed this landscape. CubeSats are miniaturized satellites built to standardized form factors (1U $\approx$ 10 cm $\times$ 10 cm $\times$ 10 cm), enabling rapid development, low-cost launch as secondary

payloads, and deployment of large constellations (HARNISCH et al., 2023). Commercial operators such as **Spire Global** and **GeoOptics** now operate CubeSat constellations that collectively provide tens of thousands of RO profiles per day, rivalling or exceeding the output of traditional government missions (BOWLER, 2020; MANNUCCI et al., 2012).

This democratization of access to RO observations creates new opportunities but also introduces significant engineering challenges. CubeSat platforms impose strict constraints on size, weight, and power (SWaP), which directly affect the design of GNSS receivers and onboard data processing systems. The limited downlink bandwidth available to small satellites often necessitates onboard data reduction, filtering, or even complete retrieval processing before transmission to ground stations (FURANO et al., 2020).

1.2 MOTIVATION: EMBEDDED ALGORITHMS FOR CUBESAT RO

A key challenge in CubeSat-based radio occultation is the development of **efficient prediction and estimation algorithms** capable of operating within the SWaP envelope of small satellite platforms. These algorithms consume pre-processed RO data—such as bending angle profiles or refractivity retrievals—and produce application-specific outputs, including:

- Atmospheric profiles (temperature, pressure, humidity) at specified vertical levels;
- Derived indices for weather or climate applications;
- Quality flags and uncertainty estimates for data assimilation.

The implementation of such algorithms on embedded hardware presents a compelling trade-off between **computational fidelity** and **resource consumption**. Two broad classes of embedded platforms are commonly considered for space applications:

1. **Microcontrollers and Microprocessors (MCU/CPU):** These offer programming flexibility and ease of development but may be limited in throughput for computationally intensive tasks.
2. **Field-Programmable Gate Arrays (FPGAs):** These reconfigurable devices can achieve high parallelism and deterministic timing, making them attractive for real-time signal processing, but they require specialized development workflows and careful management of fixed-point arithmetic (BJELOGRLIC et al., 2020).

The choice between these platforms—or hybrid architectures combining both—depends on factors such as algorithm complexity, latency requirements, power budget, and radiation tolerance. A systematic comparison of implementations across different embedded platforms is essential for informing the design of future CubeSat RO missions.

1.3 OBJECTIVES

1.3.1 General Objective

The general objective of this dissertation is to **develop, implement, and compare prediction algorithms for radio occultation data on embedded platforms**, specifically contrasting FPGA-based and microcontroller-based solutions in terms of performance, resource utilization, and energy efficiency.

1.3.2 Specific Objectives

- Conduct a comprehensive review of the state of the art in radio occultation methodology, with emphasis on CubeSat missions and onboard processing requirements.
- Define a prediction algorithm that consumes pre-processed RO data and produces atmospheric estimates suitable for near-real-time applications.
- Implement the algorithm on an FPGA platform, employing fixed-point arithmetic and high-level synthesis (HLS) techniques.
- Implement the same algorithm on a representative microcontroller or microprocessor platform.
- Develop a benchmarking framework to evaluate and compare the two implementations in terms of:
  - Prediction accuracy (RMSE, bias, correlation);
  - Computational latency and throughput;
  - Resource utilization (memory, logic cells, DSP blocks);
  - Power and energy consumption.
- Provide design guidelines for selecting embedded platforms for CubeSat RO processing based on mission requirements.

1.4 CONTRIBUTIONS

This work contributes to the field of satellite remote sensing and embedded systems by:

1. Providing a detailed methodology for adapting radio occultation retrieval algorithms to resource-constrained embedded platforms.
2. Presenting a novel comparative analysis of FPGA and microcontroller implementations for atmospheric prediction, with quantitative benchmarks.
3. Offering practical insights and design recommendations applicable to the next generation of CubeSat RO missions.

1.5 DOCUMENT STRUCTURE

This dissertation is organized as follows:

- **Chapter 2 – Methodology:** Presents the scientific foundations of radio occultation, including physical principles, measurement geometry, signal processing, inversion methods, and the role of CubeSat platforms. This chapter also describes the data sources and quality control procedures relevant to this study.
- **Chapter 3 – Prediction Algorithm:** Defines the prediction algorithm used in this work, including problem formulation, mathematical framework, and computational complexity analysis.
- **Chapter 4 – Hardware Implementation:** Describes the implementation of the algorithm on FPGA and microcontroller platforms, including design choices, optimization strategies, and development tools.
- **Chapter 5 – Results and Discussion:** Presents the experimental results, including benchmark comparisons and analysis of trade-offs between the platforms.
- **Chapter 6 – Conclusions:** Summarizes the main findings, discusses limitations, and suggests directions for future work.

2 METHODOLOGY

This chapter presents the scientific methodology underlying the radio occultation (RO) technique for atmospheric and ionospheric remote sensing. The discussion begins with the fundamental physical principles that govern the propagation of radio waves through planetary atmospheres, followed by a detailed treatment of the measurement geometry, signal processing chain, and inversion algorithms used to retrieve geophysical profiles. Particular attention is given to the emerging role of CubeSat platforms in democratizing access to high-quality RO observations, along with the associated challenges in onboard data processing that motivate the development of efficient embedded algorithms.

2.1 OVERVIEW OF THE RADIO OCCULTATION TECHNIQUE

Radio occultation is a limb-sounding technique that exploits the refraction of radio waves as they traverse a planetary atmosphere to infer vertical profiles of atmospheric properties (KURSINSKI et al., 1997; ANTHES, 2011). The technique has its origins in planetary science, where it was first employed to study the atmospheres of Mars and Venus during the Mariner and Voyager missions (FJELDBO; KLIORE; ESHLEMAN, 1971). In the terrestrial context, the advent of the Global Positioning System (GPS) and other Global Navigation Satellite Systems (GNSS) has enabled routine, high-precision atmospheric sounding on a global scale (ROCKEN et al., 1997).

The fundamental principle relies on the fact that the refractive index of the atmosphere varies with altitude due to changes in density, temperature, pressure, and water vapour content in the neutral atmosphere, as well as electron density in the ionosphere. When a radio signal from a GNSS satellite passes through the atmosphere on its way to a receiver aboard a Low Earth Orbit (LEO) satellite, the signal path is bent, and the signal experiences an excess delay relative to propagation through a vacuum (HAJJ et al., 2002). By precisely measuring these effects—specifically, the Doppler shift induced by the atmospheric bending—it is possible to retrieve vertical profiles of atmospheric refractivity, from which temperature, pressure, and humidity profiles can be derived under appropriate assumptions (KUO et al., 2004).

The key advantages of GNSS-RO for atmospheric observation include:

- **High vertical resolution:** Typical vertical resolution ranges from 0.2–1.5 km, depending on altitude and atmospheric conditions (KURSINSKI et al., 1997).
- **All-weather capability:** Unlike infrared and visible sensors, radio frequencies are

largely unaffected by clouds and precipitation, enabling continuous observations under all meteorological conditions (ANTHES, 2011).

- **Self-calibration:** The measurement is fundamentally based on timing and frequency standards traceable to atomic clocks, providing long-term stability essential for climate monitoring (STEINER et al., 2013).
- **Global coverage:** A constellation of LEO receivers can provide thousands of globally distributed profiles per day, with no geographic bias (ANTHES et al., 2008).

The technique has proven particularly valuable for numerical weather prediction (NWP), where RO observations have been shown to have a significant positive impact on forecast skill, especially in data-sparse regions such as the Southern Hemisphere oceans and polar areas (CUCURULL et al., 2007; POLI; HEALY; DEE, 2010). Furthermore, the inherent stability of RO measurements makes them an important component of the Global Climate Observing System (GCOS), providing reference-quality data for detecting long-term climate trends (STEINER et al., 2013).

2.2 CUBESAT PLATFORMS FOR RADIO OCCULTATION

The miniaturization of GNSS receiver technology and advances in CubeSat engineering have opened new opportunities for deploying radio occultation capabilities on small satellite platforms (MANNUCCI et al., 2012; HARNISCH et al., 2023). This paradigm shift has profound implications for both the scientific community and operational meteorological services, as it enables cost-effective deployment of large constellations capable of providing unprecedented spatial and temporal sampling of the atmosphere.

2.2.1 Commercial CubeSat Constellations

Several commercial operators now provide RO data from CubeSat constellations:

Spire Global operates the LEMUR constellation, consisting of more than 100 3U CubeSats equipped with multi-GNSS receivers capable of tracking GPS, GLONASS, Galileo, and QZSS signals (BOWLER, 2020). Each satellite collects atmospheric profiles using the STRATOS receiver, contributing to a daily yield of approximately 20,000 occultation profiles. Validation studies have demonstrated that Spire data quality is comparable to established missions such as COSMIC-2 (ZENG et al., 2019; GLEISNER; RASMUSSEN; FOELSCHE, 2022).

GeoOptics operates the CICERO (Community Initiative for Cellular Earth Remote Observation) constellation of 6U CubeSats (MANNUCCI et al., 2012). The CION (CICERO Instrument for GNSS-RO) receivers measure phase delays from multiple GNSS

constellations to produce atmospheric profiles, ionospheric electron density maps, and, in second-generation satellites, ocean surface measurements using GNSS-Reflectometry capabilities.

2.2.2 Advantages and Challenges of CubeSat RO

CubeSat platforms offer several advantages for radio occultation missions:

- **Reduced development cost:** CubeSat missions can be developed and deployed at a fraction of the cost of traditional satellite missions, enabling more frequent refresh cycles and technology updates (HARNISCH et al., 2023).
- **Constellation scalability:** Large numbers of CubeSats can be deployed to achieve dense spatial and temporal coverage, critical for capturing rapidly evolving atmospheric phenomena.
- **Rapid iteration:** Shorter development cycles allow for faster incorporation of technological improvements and lessons learned.

However, CubeSat platforms also present unique challenges:

- **Size, Weight, and Power (SWaP) constraints:** The limited volume (typically 1U–6U, where 1U $\approx$ 10 cm $\times$ 10 cm $\times$ 10 cm) and power budget (typically a few watts) impose stringent requirements on receiver and processing electronics (BJELOGRLIC et al., 2020).
- **Antenna limitations:** Smaller antennas may result in reduced signal-to-noise ratio, affecting the depth of penetration into the lower troposphere.
- **Onboard processing requirements:** Limited downlink capacity may necessitate significant onboard data reduction and processing, driving the need for efficient embedded algorithms—a central motivation for this thesis.

The trade-offs between processing fidelity and computational resources are particularly acute in the context of CubeSat missions, where onboard implementation of retrieval algorithms on Field-Programmable Gate Arrays (FPGAs) or microcontrollers can enable real-time or near-real-time data products while minimizing downlink requirements (FURANO et al., 2020).

2.3 GEOMETRY OF GNSS RADIO OCCULTATION MEASUREMENTS

The geometry of a GNSS-RO measurement is illustrated in Figure 1. During an occultation event, a GNSS satellite (the transmitter) sets or rises as viewed from a LEO satellite (the receiver), and the signal path passes through progressively lower (or higher) atmospheric layers. The key geometric parameters are the impact parameter a, the tangent height h_t, and the bending angle α (KURSINSKI et al., 1997; HAJJ et al., 2002).

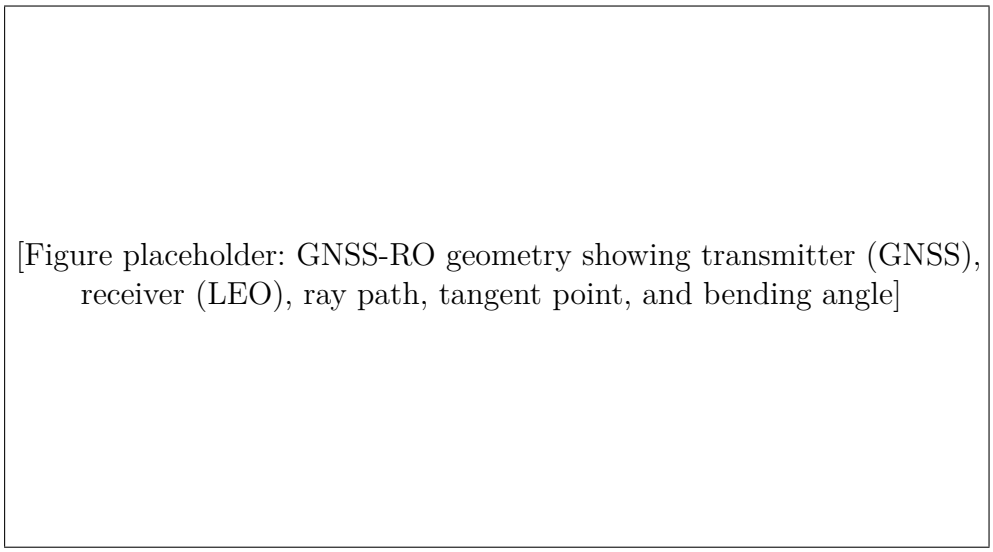

Figura 1 – Schematic geometry of a GNSS radio occultation event. The transmitted signal from the GNSS satellite is refracted as it passes through the atmosphere, arriving at the LEO receiver with a bending angle α. The tangent point represents the lowest altitude reached by the ray path. Adapted from (KURSINSKI et al., 1997).

The **impact parameter** is defined as the perpendicular distance from the centre of curvature of the atmosphere (assumed spherically symmetric) to the asymptotic straight-line extension of the ray path outside the atmosphere:

$$a = n(r) \cdot r \cdot \sin(\theta) \tag{2.1}$$

where $n(r)$ is the refractive index at radius r from the Earth's centre, and θ is the angle between the radius vector and the ray direction. Under the assumption of spherical symmetry, the impact parameter is conserved along each ray path (Snell's law in spherical geometry), which is critical for the uniqueness of the Abel inversion (BORN; WOLF, 1999).

The **bending angle** α quantifies the total angular deflection of the ray as it traverses the atmosphere. For a spherically symmetric atmosphere, it can be expressed as

an integral over the refractive index gradient:

$$\alpha(a) = -2a \int_{r_t}^{\infty} \frac{1}{\sqrt{n^2 r^2 - a^2}} \frac{d \ln n}{dr} \, dr \tag{2.2}$$

where r_t is the radial distance of the tangent point (the point of closest approach to the Earth's surface) (FJELDBO; KLIORE; ESHLEMAN, 1971). This integral equation forms the basis for retrieving the refractive index profile from the observed bending angles via the Abel transform.

A typical occultation event lasts 1–2 minutes as the tangent point descends from the mesosphere (approximately 60–80 km altitude) to the surface or until signal tracking is lost due to strong refractivity gradients in the lower troposphere (SOKOLOVSKIY, 2001). The resulting vertical profile contains information spanning a wide range of atmospheric layers, making RO a powerful tool for studying dynamics from the boundary layer to the stratosphere.

2.4 SIGNAL PROCESSING AND BENDING ANGLE RETRIEVAL

The retrieval of bending angle profiles from raw GNSS-RO observations involves several signal processing steps, each of which must be carefully executed to preserve the accuracy and precision of the final geophysical products (HAJJ et al., 2002).

2.4.1 GNSS Signal Tracking

GNSS transmitters broadcast signals on multiple frequencies—for GPS, the L1 (1575.42 MHz) and L2 (1227.60 MHz) bands are used for atmospheric sounding. The LEO receiver tracks these signals and records the carrier phase as a function of time. Two primary tracking modes are employed:

1. **Phase-Locked Loop (PLL):** In this closed-loop mode, the receiver maintains lock on the carrier signal by continuously adjusting a local oscillator to match the incoming phase. PLL tracking works well in the upper atmosphere where signal dynamics are moderate but can lose lock in the lower troposphere due to rapid phase fluctuations caused by strong refractivity gradients and multipath effects (SOKOLOVSKIY, 2001).

2. **Open-Loop (OL) Tracking:** To improve penetration into the lower troposphere, open-loop receivers record the raw signal at high sampling rates (typically 50–100 Hz) without attempting to maintain phase lock. The phase is then extracted in post-processing using spectral analysis techniques. This approach has been adopted by missions such as COSMIC and COSMIC-2 and is essential for obtaining profiles in tropical regions with strong moisture gradients (BEYERLE et al., 2005).

2.4.2 Excess Phase and Doppler Derivation

The fundamental observable in GNSS-RO is the **excess phase** ϕ_{exc}, defined as the difference between the total phase accumulated by the occulting signal and the phase that would be observed for a straight-line path through vacuum:

$$\phi_{exc}(t) = \phi_{obs}(t) - \phi_{vac}(t) \tag{2.3}$$

The excess phase arises from two contributions: the excess path length due to the refractive index ($n > 1$) and the geometric path lengthening due to ray bending. The **excess Doppler shift** is obtained by differentiating the excess phase with respect to time:

$$f_{D,exc}(t) = \frac{1}{2\pi}\frac{d\phi_{exc}}{dt} \tag{2.4}$$

This Doppler shift is directly related to the rate of change of the ray path length and, through the occultation geometry, to the bending angle.

2.4.3 Derivation of Bending Angle from Doppler

Given the positions and velocities of the GNSS and LEO satellites (obtained from precise orbit determination), the bending angle can be derived geometrically from the excess Doppler using the relation (HAJJ et al., 2002):

$$\alpha = \arcsin\left(\frac{v_{LEO}\cdot\hat{k}_{LEO}}{c} + \frac{f_{D,exc}}{f_0}\right) - \arcsin\left(\frac{v_{GNSS}\cdot\hat{k}_{GNSS}}{c}\right) - \theta_0 \tag{2.5}$$

where v_{LEO} and v_{GNSS} are the satellite velocity vectors, $\hat{k}$ denotes the ray direction vectors, f_0 is the transmitted frequency, c is the speed of light, and θ_0 is an offset angle determined by the geometry. In practice, the computation is performed iteratively since the ray directions themselves depend on the bending angle.

2.4.4 Ionospheric Correction

At the L-band frequencies used for GNSS-RO, the ionosphere contributes a significant dispersive delay that must be removed to isolate the neutral atmospheric contribution. The ionospheric refractive index at frequency f is approximately:

$$n_{iono} \approx 1 - \frac{40.3\,N_e}{f^2} \tag{2.6}$$

where N_e is the electron density in electrons per cubic metre. Because this contribution is frequency-dependent, observations at two frequencies can be combined to form an "ionosphere-free" bending angle (SYNDERGAARD, 2000):

$$\alpha_{corr} = \frac{f_1^2\,\alpha_1 - f_2^2\,\alpha_2}{f_1^2 - f_2^2} \tag{2.7}$$

Residual ionospheric errors (RIE), arising from higher-order terms and the slight spatial separation of the L1 and L2 ray paths, can introduce biases in the stratosphere, particularly during periods of high solar activity (KUO et al., 2004).

2.5 INVERSION FROM BENDING ANGLE TO ATMOSPHERIC PROFILES

The retrieval of atmospheric refractivity from observed bending angles is accomplished using the **Abel transform**, a classical integral inversion technique applicable under the assumption of local spherical symmetry (FJELDBO; KLIORE; ESHLEMAN, 1971; KURSINSKI et al., 1997).

2.5.1 The Abel Transform

Given the bending angle as a function of impact parameter, $\alpha(a)$, the refractive index (or, equivalently, refractivity $N = (n-1) \times 10^6$) can be recovered via:

$$\ln n(a_0) = \frac{1}{\pi} \int_{a_0}^{\infty} \frac{\alpha(a)}{\sqrt{a^2 - a_0^2}}\, da \tag{2.8}$$

This integral is numerically computed from the top of the profile (where $\alpha \to 0$) downward. The transformation requires knowledge of $\alpha(a)$ above the highest observation; this is typically supplied by climatological models or by a smooth exponential extrapolation.

2.5.2 Retrieval of Temperature, Pressure, and Humidity

The atmospheric refractivity at microwave frequencies is related to thermodynamic variables through the Smith-Weintraub equation (SMITH; WEINTRAUB, 1953):

$$N = \underbrace{77.6 \frac{p}{T}}_{\text{dry term}} + \underbrace{3.73 \times 10^5 \frac{e}{T^2}}_{\text{wet term}} \tag{2.9}$$

where p is the total atmospheric pressure in hPa, T is the temperature in Kelvin, and e is the partial pressure of water vapour in hPa. Above approximately 8–10 km altitude (depending on latitude and season), the water vapour contribution is negligible, and the refractivity is solely determined by the dry term. In this case, temperature can be retrieved using the hydrostatic equation and the ideal gas law, given a boundary condition (typically from a model or analysis) (KUO et al., 2004).

In the moist lower troposphere, the ambiguity between temperature and humidity contributions to refractivity requires auxiliary information for separation. This is typically achieved through:

- **One-dimensional variational (1D-Var) retrieval:** A background state from an NWP model is combined with the RO observations in a statistically optimal framework (HEALY; THéPAUT, 2006).
- **Direct assimilation:** Bending angles or refractivity are assimilated directly into NWP systems, which internally handle the temperature-humidity separation.

2.5.3 Ionospheric Electron Density Retrieval

For ionospheric studies, the same Abel inversion can be applied to the ionospheric bending angle (derived from the difference between L1 and L2 observations) to retrieve electron density profiles (SCHREINER et al., 1999):

$$N_e(h) = \frac{1}{\pi} \int_{a(h)}^{\infty} \frac{d\alpha_{iono}/da}{\sqrt{a^2 - a(h)^2}} \, da \tag{2.10}$$

These profiles provide valuable information on ionospheric structure, space weather effects, and the coupling between the neutral and ionized upper atmosphere.

2.6 DATA SOURCES AND PRE-PROCESSING

Radio occultation data are available from several operational and research missions, as summarized in Table 1.

Tabela 1 – Overview of major GNSS-RO missions and CubeSat constellations.

Mission/Constellation	Operator	Launch	Profiles/day	Platform
GPS/MET	UCAR	1995	∼150	Microsatellite
CHAMP	GFZ	2000	∼200	Microsatellite
GRACE	NASA/DLR	2002	∼200	Microsatellite
COSMIC/FORMOSAT-3	UCAR/NSPO	2006	∼2000	Microsatellite
MetOp/GRAS	EUMETSAT	2006–	∼700	Large satellite
COSMIC-2/FORMOSAT-7	UCAR/NSPO	2019	∼5000	Microsatellite
Spire LEMUR	Spire Global	2018–	∼20000	3U CubeSat
GeoOptics CICERO	GeoOptics	2018–	∼2000	6U CubeSat

Source: Compiled from (ANTHES, 2011), (HO et al., 2020), (BOWLER, 2020), and (HARNISCH et al., 2023).

Data products are typically provided at different processing levels:

- **Level 0:** Raw signal phase and amplitude measurements.
- **Level 1:** Calibrated excess phase and derived bending angle profiles as a function of impact parameter.

- **Level 2:** Retrieved geophysical profiles (refractivity, temperature, pressure, humidity, electron density).
- **Level 3:** Gridded or climatological products derived from Level 2 data.

For this thesis, the focus is on the algorithm that operates on pre-processed data (Level 1 or Level 2 products) to generate application-specific predictions or estimates.

2.7 QUALITY CONTROL AND ERROR CHARACTERIZATION

Robust quality control (QC) procedures are essential to ensure that only reliable observations are used in downstream applications. Common QC criteria include (KUO et al., 2004; SCHREINER et al., 2007):

- **Bending angle magnitude checks:** Rejection of profiles with anomalously large or small bending angles compared to climatology.
- **Smoothness criteria:** Detection of outliers based on excessive vertical gradients in bending angle or refractivity.
- **Comparison with background fields:** Statistical tests against short-range NWP forecasts to flag profiles with large departures.
- **Ionospheric residual checks:** Monitoring of the difference between L1 and L2 bending angles to identify contaminated profiles.
- **Tracking quality indicators:** Metrics such as signal-to-noise ratio and lock status to assess receiver performance.

2.7.1 Error Sources in GNSS-RO

The principal error sources affecting GNSS-RO retrievals include (KURSINSKI et al., 1997; KUO et al., 2004):

1. **Ionospheric residuals:** Despite dual-frequency correction, higher-order ionospheric terms can introduce biases of 0.1–0.5 K in retrieved temperatures in the upper stratosphere, especially during solar maximum.
2. **Multipath and atmospheric turbulence:** In the lower troposphere, strong moisture gradients can cause ray splitting (multipath) and phase fluctuations, degrading retrieval accuracy below approximately 2 km altitude.

3. **Super-refraction and ducting:** Extremely strong temperature inversions or moisture layers can trap radio waves, violating the single-ray assumption underlying the Abel inversion and causing erroneous refractivity retrievals near the surface.

4. **Orbit and clock errors:** Errors in GNSS and LEO satellite positions and clock synchronization propagate into bending angle errors, though modern precise orbit determination techniques limit these to sub-millimetre accuracy.

5. **Representativeness errors:** The RO measurement integrates information along a ray path spanning several hundred kilometres horizontally, which may not be representative of point-like radiosonde observations or NWP model grid cells (HEALY; THéPAUT, 2006).

Typical random errors (1σ) in refractivity are approximately 0.2–0.5% between 5 and 25 km altitude, increasing to 1–2% near the surface and in the upper stratosphere (SCHREINER et al., 2007; STEINER et al., 2013). Systematic errors (biases) are generally smaller but can be significant for climate applications and must be carefully characterized.

2.8 VALIDATION APPROACH

Validation of GNSS-RO products relies on comparison with independent observations and model analyses. The primary validation strategies include:

2.8.1 Radiosonde Comparisons

Collocated radiosonde observations provide the most direct validation of RO-derived temperature and humidity profiles. Standard collocation criteria typically require spatial separation of less than 200–300 km and temporal separation of less than 3 hours. Mean temperature biases of 0.1–0.3 K with standard deviations of 1–2 K are typical in the upper troposphere and lower stratosphere (SCHREINER et al., 2007). However, radiosonde observations themselves have limitations, including radiation biases, lag errors in humidity sensors, and incomplete geographic coverage.

2.8.2 Reanalysis and NWP Comparisons

Global reanalysis datasets (e.g., ERA5, MERRA-2) that do not assimilate the specific RO observations being validated can serve as independent reference fields. These comparisons are particularly valuable for assessing spatial and temporal consistency and for regions without radiosonde coverage.

2.8.3 Inter-Satellite Comparisons

Cross-comparison among different RO missions (e.g., COSMIC-2 vs. Spire vs. MetOp/GRAS) enables assessment of relative data quality and inter-mission consistency, which is critical for building long-term climate records (GLEISNER; RASMUSSEN; FOELSCHE, 2022; BOWLER, 2020).

2.8.4 Self-Consistency Tests

Internal metrics such as the agreement between ascending and descending occultations at the same location, the smoothness of retrieved profiles, and the consistency between nearby occultations can be used as additional quality indicators.

2.9 SUMMARY

This chapter has presented the scientific foundations of the radio occultation technique, from the underlying physics of atmospheric refraction to the practical aspects of signal processing, inversion, and quality control. The emergence of CubeSat constellations such as Spire and CICERO represents a transformative development in atmospheric observation, offering the potential for vastly increased data volumes at reduced cost. However, the stringent size, weight, and power constraints of CubeSat platforms create a compelling motivation for the development of computationally efficient prediction algorithms that can operate onboard these satellites, which is the central focus of the subsequent chapters of this thesis.

REFERÊNCIAS

ANTHES, R. A. Exploring Earth's atmosphere with radio occultation: contributions to weather, climate and space weather. *Atmospheric Measurement Techniques*, v. 4, n. 6, p. 1077–1103, 2011. Comprehensive review of radio occultation applications. Citado 4 vezes nas páginas 25, 29, 30 e 36.

ANTHES, R. A. et al. The COSMIC/FORMOSAT-3 mission: Early results. *Bulletin of the American Meteorological Society*, v. 89, n. 3, p. 313–333, 2008. COSMIC mission overview and early scientific results. Citado 2 vezes nas páginas 25 e 30.

BEYERLE, G. et al. GPS radio occultation with GRACE: atmospheric profiling utilizing the zero difference technique. *Geophysical Research Letters*, v. 32, n. 13, p. L13806, 2005. Zero-difference processing technique. Citado na página 33.

BJELOGRLIC, M. et al. FPGA-based embedded system design for on-board satellite processing. *Electronics*, v. 9, n. 7, p. 1175, 2020. FPGA design for satellite onboard processing. Citado 2 vezes nas páginas 26 e 31.

BORN, M.; WOLF, E. *Principles of Optics*. 7th. ed. Cambridge: Cambridge University Press, 1999. Classical optics reference for ray tracing and refraction. ISBN 978-0-521-64222-4. Citado na página 32.

BOWLER, N. E. An assessment of GNSS radio occultation data produced by Spire. *Quarterly Journal of the Royal Meteorological Society*, v. 146, n. 733, p. 3772–3788, 2020. Assessment of Spire CubeSat RO data quality. Citado 4 vezes nas páginas 26, 30, 36 e 39.

CUCURULL, L. et al. Assimilation of Global Positioning System radio occultation observations into NCEP's Global Data Assimilation System. *Monthly Weather Review*, v. 135, n. 9, p. 3174–3193, 2007. GPS-RO assimilation in NCEP GFS. Citado 2 vezes nas páginas 25 e 30.

FJELDBO, G.; KLIORE, A. J.; ESHLEMAN, V. R. The neutral atmosphere of Venus as studied with the Mariner V radio occultation experiments. *The Astronomical Journal*, v. 76, n. 2, p. 123–140, 1971. Foundational work on planetary radio occultation and Abel inversion. Citado 3 vezes nas páginas 29, 33 e 35.

FURANO, G. et al. Towards the use of artificial intelligence on the edge in space systems: challenges and opportunities. *IEEE Aerospace and Electronic Systems Magazine*, v. 35, n. 12, p. 44–56, 2020. AI and edge computing in space systems. Citado 2 vezes nas páginas 26 e 31.

GLEISNER, H.; RASMUSSEN, C. B.; FOELSCHE, U. Evaluation of radio occultation data from commercial CubeSat constellations for climate applications. *Remote Sensing*, v. 14, n. 19, p. 4991, 2022. CubeSat RO data quality for climate monitoring. Citado 2 vezes nas páginas 30 e 39.

HAJJ, G. A. et al. A technical description of atmospheric sounding by GPS occultation. *Journal of Atmospheric and Solar-Terrestrial Physics*, v. 64, n. 4, p. 451–469, 2002.

Technical description of GPS-RO signal processing. Citado 5 vezes nas páginas 25, 29, 32, 33 e 34.

HARNISCH, F. et al. The commercial radio occultation market and its benefit to numerical weather prediction. *Quarterly Journal of the Royal Meteorological Society*, v. 149, n. 755, p. 2421–2439, 2023. Commercial RO market analysis and NWP impact. Citado 4 vezes nas páginas 26, 30, 31 e 36.

HEALY, S. B.; THéPAUT, J.-N. Assimilation experiments with CHAMP GPS radio occultation measurements. *Quarterly Journal of the Royal Meteorological Society*, v. 132, n. 615, p. 605–623, 2006. Data assimilation of GPS-RO in NWP. Citado 2 vezes nas páginas 36 e 38.

HO, S.-P. et al. The COSMIC/FORMOSAT-3 radio occultation mission after 12 years: accomplishments, remaining challenges, and potential impacts of COSMIC-2. *Bulletin of the American Meteorological Society*, v. 101, n. 7, p. E1107–E1136, 2020. COSMIC-2 mission capabilities and expected impacts. Citado na página 36.

KUO, Y.-H. et al. Inversion and error estimation of GPS radio occultation data. *Journal of the Meteorological Society of Japan*, v. 82, n. 1B, p. 507–531, 2004. Comprehensive error analysis of GPS-RO retrievals. Citado 3 vezes nas páginas 29, 35 e 37.

KURSINSKI, E. R. et al. Observing Earth's atmosphere with radio occultation measurements using the Global Positioning System. *Journal of Geophysical Research: Atmospheres*, v. 102, n. D19, p. 23429–23465, 1997. Foundational paper on GPS radio occultation theory and error analysis. Citado 6 vezes nas páginas 15, 25, 29, 32, 35 e 37.

MANNUCCI, A. J. et al. CICERO: A mission to study Earth's atmosphere using GNSS occultations on a CubeSat. In: *Proceedings of the 25th International Technical Meeting of the Satellite Division of the Institute of Navigation (ION GNSS 2012)*. Nashville, TN: [s.n.], 2012. p. 3565–3573. CICERO CubeSat mission concept. Citado 2 vezes nas páginas 26 e 30.

POLI, P.; HEALY, S. B.; DEE, D. P. Assimilation of Global Positioning System radio occultation data in the ECMWF ERA-Interim reanalysis. *Quarterly Journal of the Royal Meteorological Society*, v. 136, n. 653, p. 1972–1990, 2010. GPS-RO in ERA-Interim reanalysis. Citado 2 vezes nas páginas 25 e 30.

ROCKEN, C. et al. Analysis and validation of GPS/MET data in the neutral atmosphere. *Journal of Geophysical Research: Atmospheres*, v. 102, n. D25, p. 29849–29866, 1997. First GPS/MET mission validation results. Citado na página 29.

SCHREINER, W. et al. Estimates of the precision of GPS radio occultations from the COSMIC/FORMOSAT-3 mission. *Geophysical Research Letters*, v. 34, n. 4, p. L04808, 2007. COSMIC precision estimates. Citado 2 vezes nas páginas 37 e 38.

SCHREINER, W. S. et al. Analysis and validation of GPS/MET radio occultation data in the ionosphere. *Radio Science*, v. 34, n. 4, p. 949–966, 1999. Ionospheric electron density retrieval from GPS-RO. Citado na página 36.

SMITH, E. K.; WEINTRAUB, S. The constants in the equation for atmospheric refractive index at radio frequencies. *Proceedings of the IRE*, v. 41, n. 8, p. 1035–1037, 1953. Foundational refractivity equation for atmospheric applications. Citado na página 35.

SOKOLOVSKIY, S. V. Tracking tropospheric radio occultation signals from low Earth orbit. *Radio Science*, v. 36, n. 3, p. 483–498, 2001. Open-loop tracking for tropospheric RO. Citado na página 33.

STEINER, A. K. et al. Quantification of structural uncertainty in climate data records from GPS radio occultation. *Atmospheric Chemistry and Physics*, v. 13, n. 3, p. 1469–1484, 2013. Structural uncertainty quantification in GPS-RO climate records. Citado 3 vezes nas páginas 25, 30 e 38.

SYNDERGAARD, S. On the ionosphere calibration in GPS radio occultation measurements. *Radio Science*, v. 35, n. 3, p. 865–883, 2000. Ionospheric correction methods for GPS-RO. Citado na página 34.

WICKERT, J. et al. Atmosphere sounding by GPS radio occultation: First results from CHAMP. *Geophysical Research Letters*, v. 28, n. 17, p. 3263–3266, 2001. CHAMP mission first results. Citado na página 25.

ZENG, Z. et al. GPS RO refractivity bias correction for N W P applications: preliminary results from Spire data. *Atmospheric Measurement Techniques Discussions*, 2019. Spire data bias correction for NWP. Citado na página 30.